CHEMISTRY OF MATERIALS

pubs.acs.org/cm Article

Thermal Atomic Layer Etching of Molybdenum Using Sequential Oxidation and Deoxychlorination Reactions

Taewook Nam, Troy A. Colleran, Jonathan L. Partridge, Andrew S. Cavanagh, and Steven M. George*

Cite This: Chem. Mater. 2024, 36, 1449−1458 Read Online

ABSTRACT: Thermal atomic layer etching (ALE) of molybdenum (Mo) was demonstrated using sequential exposures of O_3 (ozone) and $SOCl_2$ (thionyl chloride). In situ quartz crystal microbalance (QCM) studies were performed on sputtered Mo-coated QCM crystals. The QCM results revealed that Mo ALE displayed a linear mass decrease versus ALE cycles after a short etching delay. A pronounced mass increase was observed for every O_3 exposure. A dramatic mass decrease occurred for every $SOCl_2$ exposure. The mass change per cycle (MCPC) for Mo ALE was self-limiting after long $SOCl_2$ exposures. The MCPC increased slightly with longer O_3 exposure times. In situ QCM studies suggested that this soft saturation with longer exposure to the O_3 resulted from the diffusion-limited oxidation of Mo. The Mo etch rate increased progressively with etching temperature. Under saturation conditions, the Mo etch rates were 0.94, 5.77, 8.83, and 10.98 Å/cycle, at 75, 125, 175, and 225 °C, respectively. X-ray photoelectron spectroscopy (XPS) and in situ quadruple mass spectroscopy (QMS) studies were conducted to understand the reaction mechanism. XPS revealed primarily MoO_3 on the Mo surface after exposure to O_3 at 150 °C. From the QMS studies, volatile SO_2 and MoO_2Cl_2 were monitored when Mo was exposed to $SOCl_2$ during the ALE cycles at 200 °C. These results indicate that Mo ALE occurs via oxidation and deoxychlorination reactions. Mo is oxidized to MoO_3 by O_3. Subsequently, MoO_3 undergoes a deoxychlorination reaction where $SOCl_2$ accepts oxygen to yield SO_2 and donates chlorine to produce MoO_2Cl_2. Additional QCM experiments revealed that sequential exposures of O_3 and SO_2Cl_2 (sulfuryl chloride) did not etch Mo at 250 °C. Time-resolved QMS studies at 200 °C also compared sequential O_3 and $SOCl_2$ or SO_2Cl_2 exposures on Mo at 200 °C. The volatile release of MoO_2Cl_2 was observed only using the $SOCl_2$ deoxychlorination reactant. Atomic force microscopy (AFM) measurements revealed that the roughness of the Mo surface increased slowly versus Mo ALE cycles.

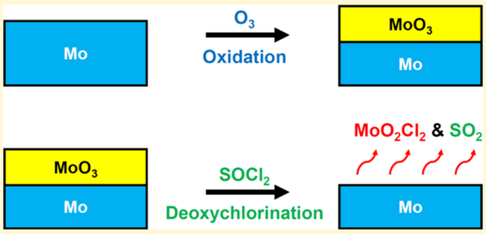

I. INTRODUCTION

Thermal atomic layer etching (ALE) has emerged as a promising technique for atomic layer-controlled removal of material.[1,2] Thermal ALE is based on sequential, gas phase, self-limiting surface reactions.[2] The first thermal reaction involves modification of the top layer of the material surface. The second thermal reaction then leads to the volatilization of the modified surface layer.[2] Thermal ALE leads to isotropic etching because gaseous reactants can access the entire surface area of complex three-dimensional and high-aspect-ratio structures.[1,2] In comparison, plasma ALE utilizes high-energy ions to volatilize the modified surface layer.[3] Plasma ALE leads to anisotropic etching because the collision of the directional ions with the surface requires line-of-sight.[3]

Thermal ALE has developed rapidly since the discovery of Al_2O_3 thermal ALE in 2015.[4] The thermal ALE of metal oxides and metal nitrides typically involves fluorination for surface modification and then ligand exchange for volatilization of the modified surface layer.[2,5] Examples of the fluorination and ligand exchange mechanism for a variety of materials include Al_2O_3,[4,6−9] HfO_2,[7,10−12] ZrO_2,[7,12−14] Ga_2O_3,[15] GaN,[16] and AlN.[17,18]

Conversion of the initial material to a different material can also play a role in the thermal ALE of SiO_2,[19] ZnO,[20] VO_2,[21] and Al_2O_3.[22] Oxidation of metal nitrides to metal oxides can also facilitate the etching of nitrides such as TiN.[23] Semiconductor materials, such as Si,[24] SiGe,[25] and Si_3N_4,[26] can also undergo thermal ALE through oxidation, conversion, and fluorination and ligand exchange mechanisms. Metal fluorides, such as AlF_3,[27] and metal sulfides, such as ZnS,[28] can also be etched by thermal ALE processes.

The thermal ALE of elemental metals has also progressed in recent years. Initial studies developed W ALE using an oxidation, conversion, and volatile release process using O_2, BCl_3, and HF reactants.[29] Additional processes for W ALE involved oxidation followed by fluorination or chlorination with WF_6 or WCl_6, respectively, to release volatile W oxyfluorides or oxychlorides.[30,31] Ni and Co ALE processes were subsequently developed based on chlorination and ligand addition mechanisms.[32,33] Chlorination was accomplished using SO_2Cl_2 and

Received: October 11, 2023
Revised: December 12, 2023
Accepted: December 22, 2023
Published: January 29, 2024

https://doi.org/10.1021/acs.chemmater.3c02606
Chem. Mater. 2024, 36, 1449−1458

ligand addition to release a volatile product was achieved using L-ligands such as $P(CH_3)_3$ or tetramethylethylenediamine (TMEDA).[32,33]

Other metal ALE pathways have been designed using hexafluoroacetylacetone (Hhfac) for the volatilization of either oxidized or halogenated metals. Cu ALE was achieved using O_2 or O_3 for oxidation and Hhfac for volatile release.[34] Co ALE was also accomplished using chlorination by Cl_2 and volatilization using ligand substitution and hydrogen transfer reactions with Hhfac.[34−36] The oxidation-based metal ALE strategies have their origin in earlier studies of the spontaneous etching of Cu oxides using Hhfac exposures.[37−40] Additional metal etching has utilized oxidation using an O_2 plasma followed by volatilization of the oxidized metal layer using other organic precursors such as formic acid.[41]

Molybdenum (Mo) is a refractory metal used to form metal alloys that have high strength and resistance against corrosion.[42] Mo has also been targeted by the semiconductor industry as a possible candidate for sub-10 nm interconnects because of its small electron mean free path compared with other metals.[43,44] Etching processes for Mo can involve high-temperature sublimation,[45] wet etching,[46] or plasma-based etching.[47,48] Plasma-based Mo ALE processes have also been developed recently using oxidation and chlorination or fluorination to form volatile oxychlorides or oxyfluorides.[49,50] However, there have been no previous reports of a Mo thermal ALE process. Thermal ALE processes are desirable because they avoid the ion surface damage that can occur during plasma processing. Likewise, thermal ALE processes are isotropic and yield atomic scale etching control.

In this paper, the thermal ALE of Mo was studied by in situ quartz crystal microbalance (QCM) and quadruple mass spectrometry (QMS) measurements using oxidation and deoxychlorination reactions. Ozone (O_3) was used as the oxidation reactant. Thionyl chloride ($SOCl_2$) was employed as the deoxychlorination reactant. The etch rate of Mo ALE was characterized versus reactant exposure times and process temperatures. XPS measurements were used to determine the oxidation state of Mo after O_3 exposure. QMS analysis identified the volatile products that were produced during reactant exposures. The surface morphology versus ALE cycles was also measured by atomic force microscopy (AFM) to determine if thermal ALE roughens the surface. Additional studies compared the differences between the $SOCl_2$ and sulfuryl chloride (SO_2Cl_2) reactants for thermal Mo ALE.

II. EXPERIMENTAL SECTION

The thermal ALE experiments were conducted in a viscous flow hot wall reactor. The configuration of this reactor is similar to a reactor that has been reported previously.[51] The reactor was heated using ceramic heaters (VS102A06S, VS102A12S, Watlow). To maintain a constant process temperature for the QCM measurements, the reactor temperature was controlled using a proportional-integral-derivative (PID) temperature controller (Nanodac, Eurotherm) and a power controller (EPack, Eurotherm). These controllers maintained the reactor temperature within a range of ±0.1 °C. The reactor was pumped with a mechanical rotary vane pump (2010C1, Pfeiffer). The base pressure of the reactor was maintained at 20 mTorr without gas flow and 1 Torr with a constant flow of ultrahigh-purity (UHP)-grade nitrogen (N_2) gas (99.999%, Airgas).

The Mo thin films used for the Mo ALE experiments were grown on p-type silicon (Si) wafers (Silicon Valley Microelectronics, Inc.) and gold-coated quartz crystals (TAN06RCGP, Phillips Technologies) using DC magnetron sputtering (TORUS Mag Keeper Circular Magnetron Sputtering Sources, Kurt J. Lesker). For this physical vapor deposition (PVD), the purity of the Mo sputtering target was 99.95% (Kurt J. Lesker). The base pressure of the sputtering chamber was below 5×10^{-8} Torr. For sputtering, Ar was introduced to the chamber to define a working pressure of 5 mTorr. The plasma power was delivered from a power supply (PD500X3, Kurt J. Lesker) and the power was fixed at 25 W. To obtain high-purity Mo PVD, 10 min of pre-sputtering was conducted prior to sample deposition. For uniform film deposition, the substrate holder was rotated during PVD at a speed of 30 rpm.

For Mo etching, O_3 was used as the oxidizing agent and SO_2Cl_2 (97%, Millipore Sigma) and $SOCl_2$ (99.5%, Millipore Sigma) were explored as chlorination reactants. O_3 was produced from an O_3 generator (OG-60H, TMEiC) using UHP grade oxygen (O_2) (99.999%, Airgas). The O_3 concentration was 200 g/m^3 with 1 L/min of O_2 flow. Both SO_2Cl_2 and $SOCl_2$ precursors were supplied from glass canisters and maintained at room temperature (∼25 °C). The pressure of O_3/O_2 was 1 Torr. SO_2Cl_2 and $SOCl_2$ were both exposed at a pressure of 200 mTorr.

The mass change of the Mo film during the ALE process was monitored by an in situ QCM.[51] After a Mo film was deposited on a gold-coated QCM crystal, the crystal was mounted inside of a Cool Drawer Single Sensor housing (CDS-A1F47-15, Inficon). The sensor housing was sealed using a low-outgassing, high-temperature epoxy (Epo-Tek H21D, Epoxy Technology, Inc.). The epoxy was cured at ∼60 °C for more than 12 h to avoid backside deposition and corrosion of the internal components.[51] After the crystal was loaded into the drawer, the QCM sensor was mounted within the isothermal region of the reactor. All of the QCM measurements during Mo ALE were recorded by a high-resolution thin-film deposition monitor (SQM-160-H-2-E, Inficon). The thickness resolution of the QCM monitor to Mo was ∼0.037 Å.

X-ray photoelectron spectroscopy (XPS) (PHI 5600, Physical Electronics) was utilized to determine the oxidation states of Mo before and after O_3 exposure. A monochromatic Al Kα X-ray source (1486.6 eV) was used to collect scans with a pass energy of 93.9 eV and a step size of 0.400 eV. Surface survey scans were performed without Ar$^+$ sputtering to observe the surface oxidation states after O_3 exposures. All XPS spectra were calibrated using the adventitious C 1s XPS peak at 284.6 eV.[52] Survey scans of as-deposited Mo were performed with and without 3 keV Ar$^+$ ion sputtering. CasaXPS software (Casa Software Ltd.) was utilized to analyze the XPS spectra. The data fitting and deconvolution employed Shirley backgrounds and Gaussian−Lorentzian functions.[53]

The QMS studies were performed in a custom-built reactor using a Mo powder sample. A detailed description of this reactor has been given previously.[54,55] The two reactant lines were isolated until the reactants arrived at the Mo powder bed. The Mo powder (99.9%, average particle size ∼35−45 nm, US Research Nanomaterials, Inc.) was housed in a stainless-steel enclosure with a stainless-steel mesh. The etching of Mo powder was conducted at 200 °C. The Mo powder housing was left in the reactor for at least 12 h prior to the reactant exposures to remove adsorbed water from the Mo powder.

The volatile etch products were formed in a N_2 background gas at a pressure of ∼1.5 Torr in the sample holder. The partial pressure of each reactant was approximately 1 Torr. A fraction of the N_2, and the reactant and product gases, expanded through an aperture into a low-pressure differentially pumped region to form a molecular beam.[55] The products in the molecular beam then passed through a skimmer into a second differentially pumped region that housed the quadrupole mass spectrometer (Extrel, MAX-QMS Flanged Mounted System).[55] An electron ionization energy of 70 eV was used for the QMS experiments. To minimize exposure to corrosive gases, the ionizer and analyzer were positioned perpendicular to the incoming molecular beam.

An atomic force microscope (AFM) (NX-10, Park Systems) was utilized to characterize the surface roughness of the Mo film deposited on a Si coupon substrate before and after Mo ALE. The AFM images were recorded using noncontact mode (NCM) with a scan rate of 1 Hz and a stage-mounted PPP-NCHR (Nanosensors) probe. After image acquisition, various parameters from the AFM image were derived using XEI software (Park Systems).

To characterize the crystallinity and density of the Mo film, grazing incidence X-ray diffraction (GI-XRD) and X-ray reflectivity (XRR) were conducted using an X-ray diffractometer (Bede D1, Jordan Valley Semiconductors). These measurements employed radiation from Cu Kα at λ = 1.54 Å. The X-ray tube filament voltage and current were 40 kV and 35 mA, respectively. The incident angle of the X-rays for the XRD scans was 0.3°. The XRD scans were analyzed using Jordan Valley Polycrystal (Jordan Valley Semiconductors). The XRR scans were fit using Bede REFS software (Jordan Valley Semiconductors).

III. RESULTS AND DISCUSSION

III.I. QCM Measurements of Mo ALE Using O_3/SO_2Cl_2 and $O_3/SOCl_2$. Figure 1 shows the mass change during 70 cycles of sequential exposures of the O_3/SO_2Cl_2 and the $O_3/SOCl_2$ on the Mo-coated QCM crystals at 250 °C, respectively. For these studies prior to establishing the saturation conditions, the O_3 and chlorine reactant times were initially set to 1 and 2 s, respectively. The purge time was 120 s after both the O_3 exposure and chlorine reactant exposure. This reaction sequence can be designated as (1, 120, 2, 120) where the numbers indicate the reactant or purge times in seconds. Figure 1 reveals that there is negligible mass change when O_3 and SO_2Cl_2 were sequentially exposed to the Mo film for 70 cycles.

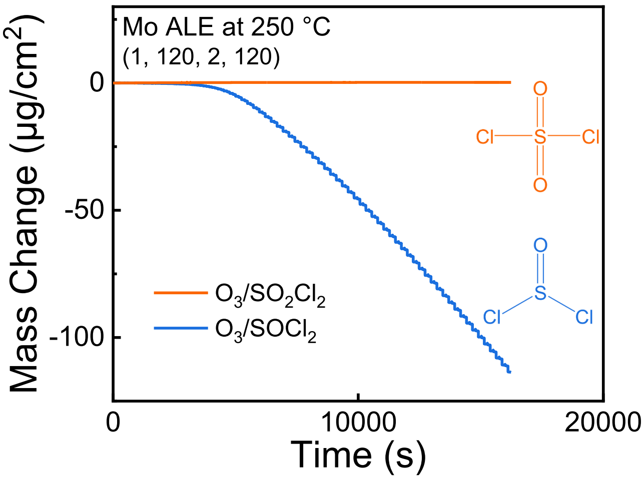

Figure 1. Mass change versus time for Mo ALE using sequential O_3/SO_2Cl_2 and $O_3/SOCl_2$ exposures at 250 °C with (1, 120, 2, 120) reaction sequence.

In contrast, Figure 1 shows that a linear mass decrease was monitored for sequential exposure to O_3 and $SOCl_2$ after a short delay. This linear mass decrease indicates Mo etching by sequential O_3 and $SOCl_2$ exposures. The mass change per cycle (MCPC) was −2710.7 ng/(cm^2 cycle). The corresponding Mo etch rate of −2.7 nm/cycle was calculated using the MCPC and the mass density for the Mo PVD film of 10.11 g/cm^3. This mass density was derived from XRR measurements. Note that this initial experiment comparing the SO_2Cl_2 and $SOCl_2$ chlorine reactants was not conducted under saturation conditions.

Given the results in Figure 1, the proposed etching mechanism during Mo ALE using O_3 and $SOCl_2$ can be depicted as shown in Figure 2. The proposed chemical reactions during Mo ALE can be written as

$$Mo + O_3(g) \rightarrow MoO_x + O_2(g) \quad (1)$$

$$MoO_x + SOCl_2(g) \rightarrow MoO_yCl_z(g) + SO_2(g) \quad (2)$$

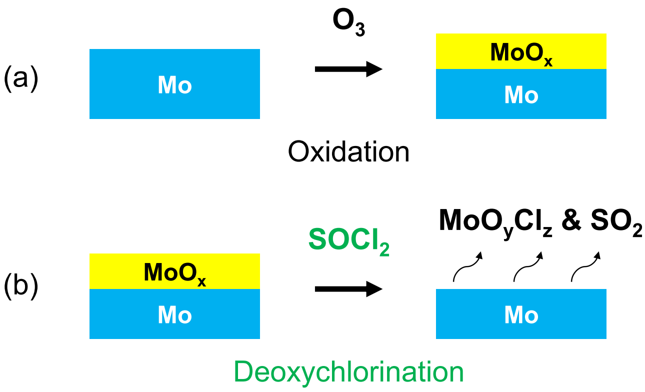

Figure 2. Proposed etching mechanism for Mo thermal ALE using sequential O_3 and $SOCl_2$ exposures.

Mo is first oxidized by reaction with O_3. Subsequently, MoO_x produces volatile MoO_yCl_z oxychloride products after the reaction with $SOCl_2$. The absence of Mo etching with SO_2Cl_2 suggests that $SOCl_2$ acts as a deoxychlorination reactant. $SOCl_2$ can accept oxygen from MoO_x and donate chlorine to yield SO_2 as a reaction product. In contrast, SO_2Cl_2 may not be etching Mo because SO_2Cl_2 is not an effective oxygen acceptor.

Mo has different oxidation states depending on the oxidation conditions.[56,57] The oxidation state of Mo after O_3 exposure can be estimated using thermochemical predictions for the standard Gibbs free energy change.[58] At 175 °C, Mo oxidation by O_3 could occur according to

$$Mo + 4/3O_3(g) \rightarrow MoO_2 + O_2(g) \quad \Delta G^\circ = -175.9\ \text{kcal} \quad (3)$$

$$Mo + 5/3O_3(g) \rightarrow MoO_3 + O_2(g) \quad \Delta G^\circ = -219.1\ \text{kcal} \quad (4)$$

MoO_3 may be the dominant Mo oxide after exposure to O_3 because eq 4 has the largest negative standard Gibbs free energy change.

Assuming MoO_3 is the Mo oxide formed by O_3 exposure, the predicted reactions between MoO_3 and $SOCl_2$ at 175 °C can be written as

$$MoO_3 + 2SOCl_2(g) \rightarrow MoOCl_4(g) + 2SO_2(g) \quad \Delta G^\circ = -18.0\ \text{kcal} \quad (5)$$

$$MoO_3 + SOCl_2(g) \rightarrow MoO_2Cl_2(g) + SO_2(g) \quad \Delta G^\circ = -15.0\ \text{kcal} \quad (6)$$

Either $MoOCl_4$ or MoO_2Cl_2 could be the volatile etch product because the standard Gibbs free energy changes are very similar for eqs 5 and 6.

The Mo etch rate during Mo ALE was then measured as a function of precursor exposure time to determine the conditions for self-limiting reactions. Figure 3 shows the MCPC for Mo ALE with different O_3 and $SOCl_2$ exposure times at 150 °C. The saturation of the MCPC or etch rate for Mo ALE was obtained when the O_3 and $SOCl_2$ exposure times were 2 and 5 s, respectively. The purge times were 120 s after the O_3 and $SOCl_2$ exposures. At saturation at 150 °C, the MCPC and Mo etch rates were 770 ng/(cm^2 cycle) and 7.6 Å/cycle, respectively.

https://doi.org/10.1021/acs.chemmater.3c02606

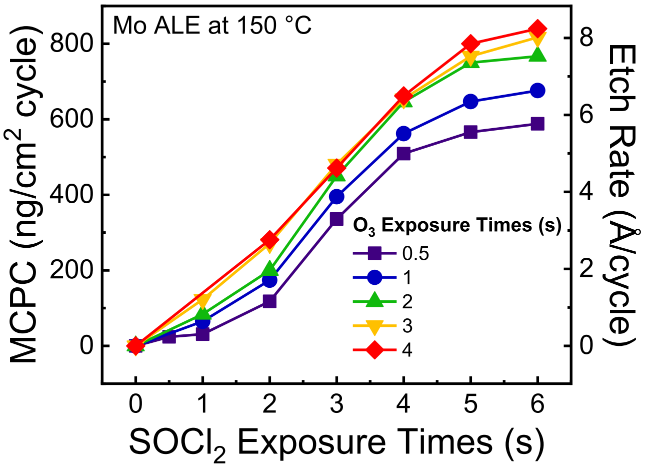

Figure 3. Mass change per cycle (MCPC) and etch rates for Mo ALE at 150 °C versus O_3 and $SOCl_2$ exposure times.

Figure 3 shows that the MCPC increases slightly with O_3 exposure time. This slow saturation may be related to the diffusion-limited oxidation of Mo according to a Deal−Grove mechanism.[59] Once the Mo oxide is formed by O_3, the oxide layer acts as a diffusion barrier that slows but does not completely prevent further Mo oxidation. Consequently, Mo ALE shows a slow saturation of the MCPC with increasing O_3 exposure times.

To confirm the diffusion-limited Deal−Grove oxidation of Mo, the Mo surface was exposed to 10 $SOCl_2$ exposures. Subsequently, this chlorinated surface was exposed to O_3/O_2 at 30 mTorr for 1800 s. Figure 4a shows the mass change during the O_3 exposure. The mass initially shows a small decrease versus O_3 exposure for the first 7 s. An expansion of Figure 4a displaying the first 40 s of the exposure to O_3 is shown in Figure 4b. The initial mass decrease for the first 7 s may be caused by the reaction of O_3 with the chlorinated Mo surface and formation of volatile Mo oxychloride species.

Figure 4b shows that the mass increases from 7 to 40 s. This mass increase coincides with the oxidation of the Mo substrate. Figure 4a reveals that the Mo oxidation is fairly linear up to 200 s. Subsequently, the mass continues to increase at a progressively slower rate from 200 to 1800 s. The mass gain is parabolic and consistent with a diffusion-limited growth regime.[60] The formation of an oxide layer forms a diffusion barrier that slows the oxidation of the underlying Mo film. This behavior is consistent with the weak saturation of the MCPC observed in Figure 3.

Figure 5 shows the Mo mass change during sequential O_3 and $SOCl_2$ exposures at 150 °C under the saturation conditions obtained from Figure 3. The O_3 and $SOCl_2$ exposure times were 2 and 5 s, respectively. The purge times were 120 s after both the O_3 exposure and chlorine reactant exposure. There is a delay during the first 13 ALE cycles prior to reaching the linear etch region. A constant mass decrease per ALE cycle is monitored in the linear etch region.

An expansion of Figure 5 in the linear regime is shown in Figure 6. The QCM measurements observed digital mass changes during sequential O_3 and $SOCl_2$ exposures. There is a pronounced mass gain of $\Delta M_{O_3} = +111.9$ ng/cm^2 during the O_3 exposures. Likewise, there is a distinct mass loss of $\Delta M_{SOCl_2} = -895.5$ ng/cm^2 during the $SOCl_2$ exposures. The MCPC for Mo ALE at 150 °C was −783.6 ng/(cm^2 cycle). These mass changes also support the proposed etching mechanism for Mo ALE presented in Figure 2. During the O_3 exposure, Mo is oxidized

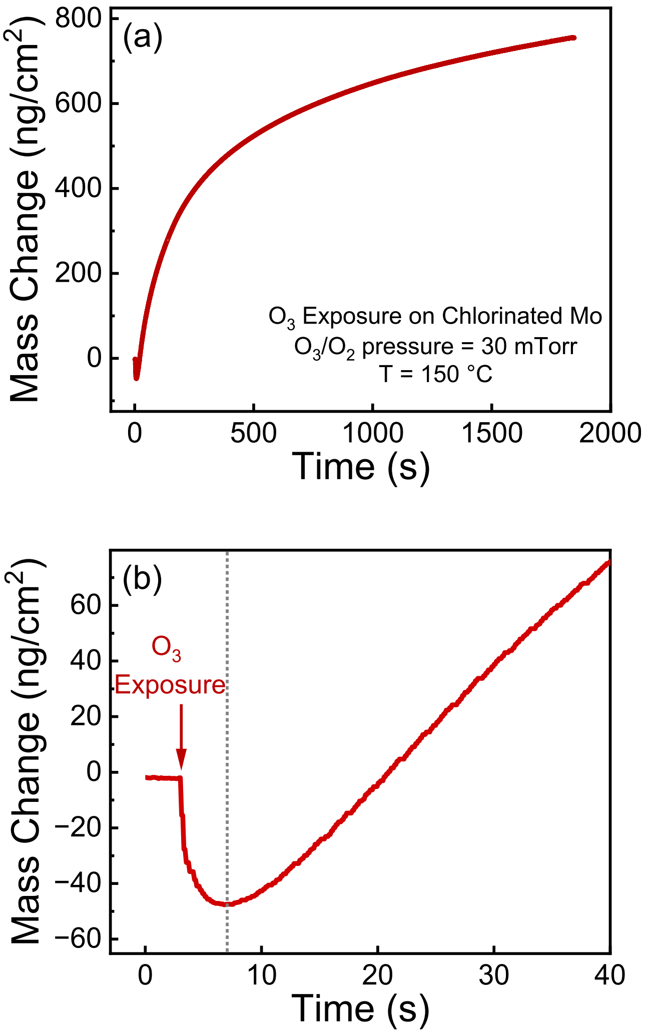

Figure 4. Mass change during oxidation of Mo at 150 °C with O_3/O_2 pressure at 30 mTorr for (a) times from 0 to 1800 s and (b) times from 0 to 40 s.

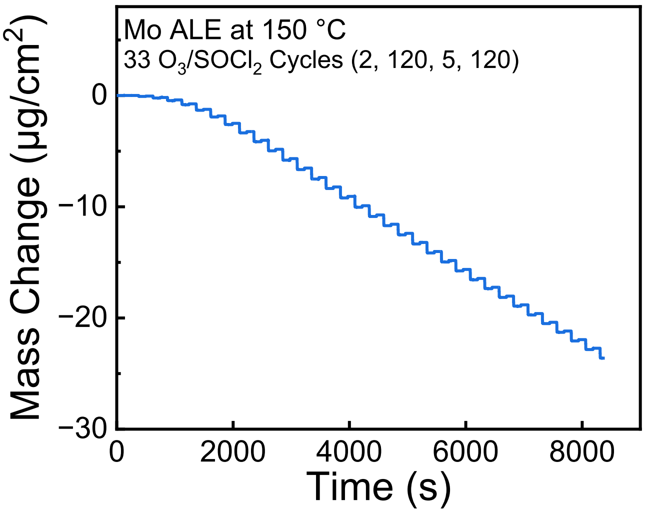

Figure 5. Mass change for Mo thermal ALE at 150 °C using sequential O_3 and $SOCl_2$ exposures with a (2, 120, 5, 120) reaction sequence under saturation conditions.

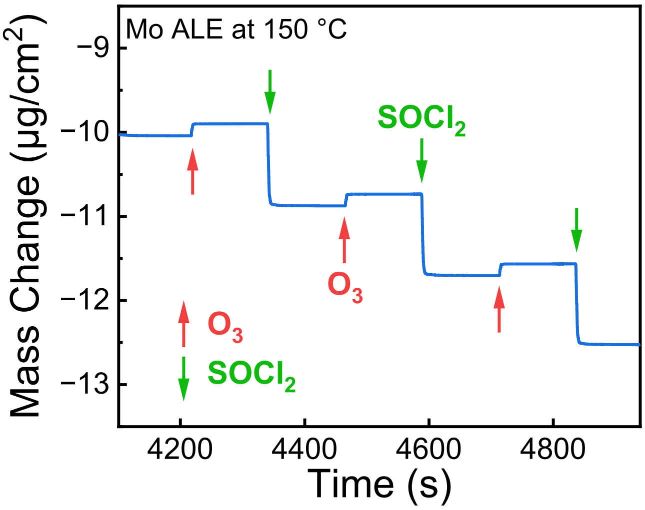

Figure 6. Enlargement of mass change for Mo ALE at 150 °C in the linear mass decrease regime shown in Figure 5.

and forms MoO_x on the surface, leading to mass increase. During $SOCl_2$ exposure, the surface MoO_x layer is removed by forming volatile products from the reaction between $SOCl_2$ and MoO_x. This removal of the MoO_x layer produced a mass loss.

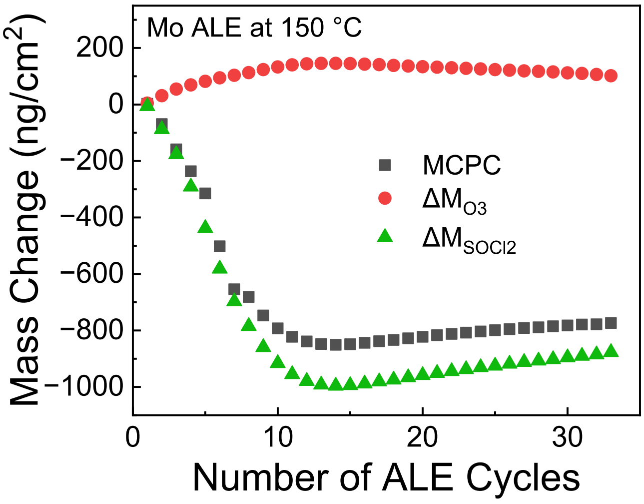

Figure 7. Mass changes after individual O_3 exposures (ΔM_{O_3}), $SOCl_2$ exposures (ΔM_{SOCl_2}), and total mass change per cycle (MCPC) for Mo ALE at 150 °C.

Figure 7 shows the mass changes during Mo ALE after the O_3 exposures (ΔM_{O_3}), after the $SOCl_2$ exposures (ΔM_{SOCl_2}), and the resulting MCPC at 150 °C. These results are from the QCM results in Figure 5. The delay before reaching the linear etch regime is clearly observed during the first 13 ALE cycles. After 13 ALE cycles, the mass changes are much more constant over the next 20 ALE cycles. The delay may be caused by the initial oxide layer on the Mo film.

Figure 8 shows the mass change during Mo ALE at different etching temperatures under saturation conditions using the reaction sequence (2, 120, 5, 120). The etching temperatures varied from 75 to 225 °C. The time required for the QCM to stabilize at each new temperature was ∼6 h. All of the results were extracted from the linear etch region during Mo ALE. The time origins have been displaced at each temperature to exclude the delays to reach the linear etch region. The delays were shorter at higher temperatures.

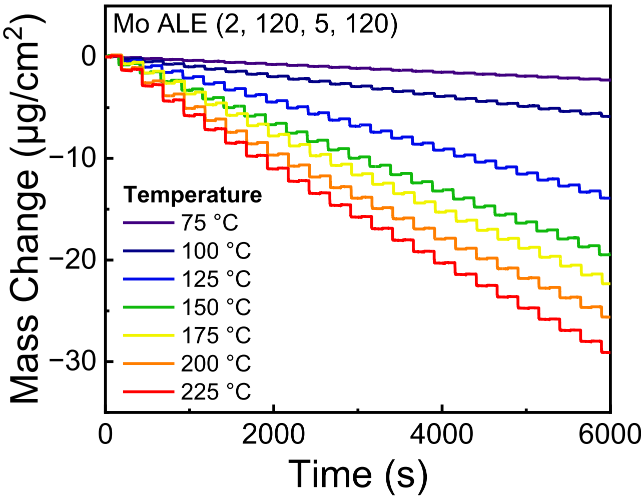

Figure 8. Mass change versus time for Mo thermal ALE using sequential O_3 and $SOCl_2$ exposures at different temperatures with a (2, 120, 5, 120) reaction sequence under saturation conditions.

The delays in reaching the linear etch region were believed to result from surface oxidation during temperature stabilization. Independent experiments at higher temperatures confirmed that sequential $SOCl_2$ exposures on the Mo surface after temperature stabilization led to mass decreases that became progressively smaller with the number of $SOCl_2$ exposures. These results suggest that $SOCl_2$ can eventually remove the oxide layer formed during temperature stabilization. In addition, the oxidation state of the oxide layer formed during temperature stabilization may be different from the oxidation state formed by O_3.

A stepwise mass decrease is observed versus ALE cycles for every temperature. The MCPC values were −96, −245, −588, −786, −900, −985, and −1119 ng/(cm^2 cycle) at 75, 100, 125, 150, 175, 200, and 225 °C, respectively. These MCPC values correspond to etch rates of 0.9, 2.4, 5.8, 7.7, 8.8, 9.7, and 11.0 Å/cycle, respectively. The increase in the MCPC with the temperature indicates a thermally activated process.

III.II. XPS Measurements of Mo Surface before and after O_3 Exposures. Figure 9a shows the XPS spectra of the as-deposited Mo film and the Mo film after O_3 exposure at 150 °C. The XPS spectrum for the as-deposited Mo film was consistent with binding energies for Mo^0, Mo^{4+}, Mo^{5+}, and Mo^{6+}.[52,61] Compared with the as-deposited Mo spectrum, the XPS spectrum after O_3 exposure was shifted to higher binding energies. Survey spectra of the as-deposited Mo film and the as-deposited Mo film after Ar^+ sputtering are given in Figure S1 in the Supporting Information.

The deconvolution of the XPS spectrum after exposure to O_3 is displayed in Figure 9b. The two dominant peaks located at 232.3 and 235.4 eV correspond to Mo^{6+} $3d_{5/2}$ and Mo^{6+} $3d_{3/2}$, respectively.[61] A smaller peak is also visible at 227.7 eV. This peak is assigned to Mo^0 $3d_{5/2}$ that exists below the oxide layer.[61] These results are consistent for MoO_3 as the Mo oxide that is formed by O_3 exposures. MoO_3 also matches the thermochemical predictions from eq 4.

III.III. Mass Spectrometry Studies of Thermal Mo ALE. QMS experiments were performed to identify the volatile

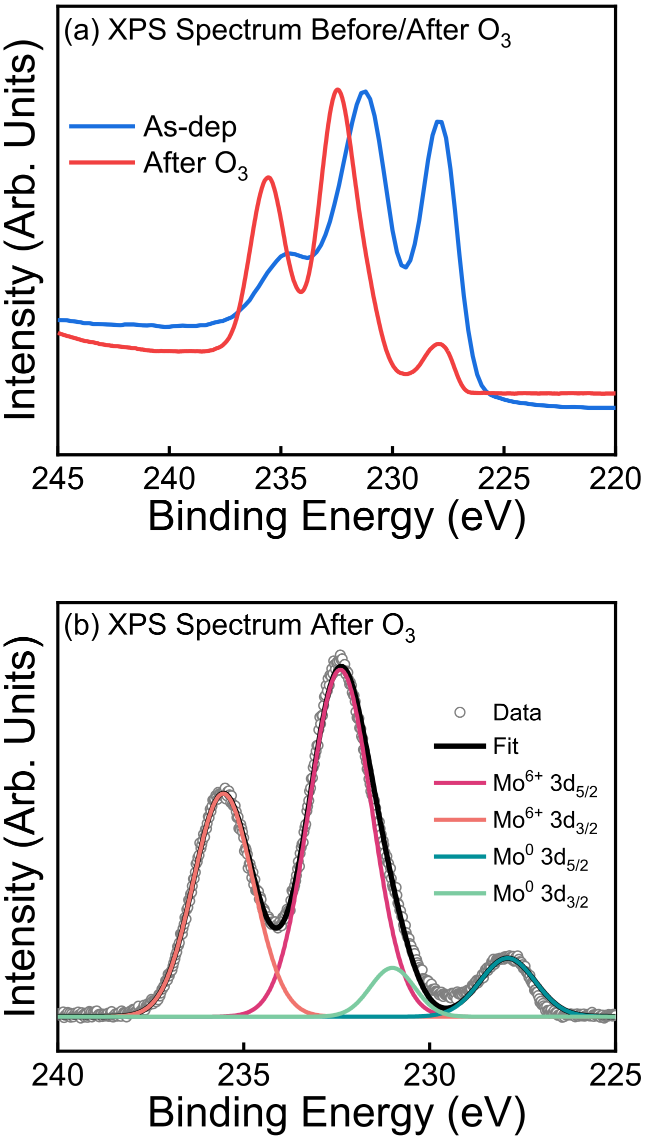

Figure 9. (a) XPS spectra in Mo 3d region before and after O_3 exposure and (b) deconvoluted XPS spectrum after O_3 exposure at 150 °C.

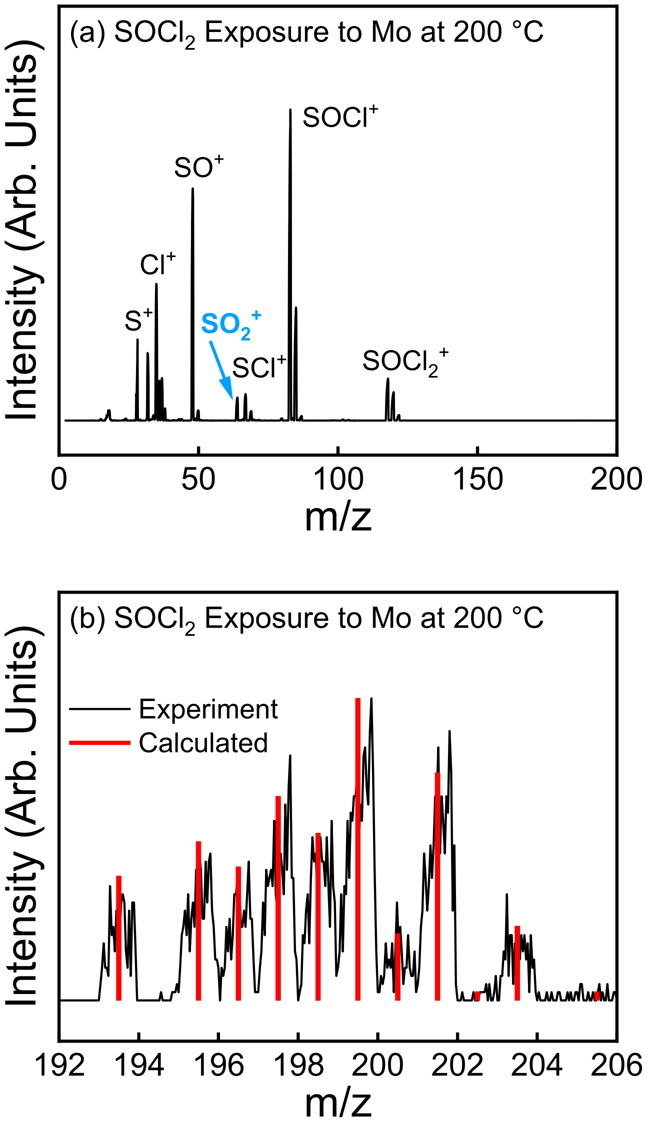

Figure 10. QMS spectra during $SOCl_2$ exposure for Mo thermal ALE on Mo powder using sequential O_3 and $SOCl_2$ exposures at 200 °C in two different mass regions: (a) m/z 5−200 and (b) m/z 192−206.

etching products during Mo ALE using exposures of O_3 and $SOCl_2$ to Mo powder at 200 °C. Figure 10 displays the ion signal intensities during the $SOCl_2$ exposure during the fourth ALE cycle over two different ranges of m/z values: (a) 5−200; and (b) 192−206. Figure 10a shows that most of the ion signals in the range from m/z 5 to 200 were attributed to the $SOCl_2^+$ parent ion and its cracking fragments. During $SOCl_2$ exposure, S^+, Cl^+, SO^+, SCl^+, $SOCl^+$, and $SOCl_2^+$ ion signal intensities were monitored at m/z 32, 35, 48, 67, 83, and 118, respectively. These ion signal intensities match the mass spectrum of $SOCl_2$ reported earlier.[62] However, the ion signal located at m/z 64 corresponds to SO_2^+. This ion signal for SO_2^+ is produced by the reaction between $SOCl_2$ and MoO_3.

Figure 10b shows the ion signals for $MoO_2Cl_2^+$ that were monitored in the mass range from m/z 192 to 206. These ion signal intensities for $MoO_2Cl_2^+$ closely match the calculated MoO_2Cl_2 signal intensities based on the natural isotopic abundances. Mo has seven stable isotopes: ^{92}Mo (15.86%), ^{94}Mo (9.12%), ^{95}Mo (15.70%), ^{96}Mo (16.50%), ^{97}Mo (9.45%), ^{98}Mo (23.75%), and ^{100}Mo (9.62%).[63] Cl has two stable isotopes: ^{35}Cl (75.77%) and ^{37}Cl (24.23%). These stable isotopes and their natural abundances produce the calculated ion intensities in Figure 10b.

The excellent agreement between the observed ion signal intensities and the calculated ion signal intensities based on the natural isotopic abundances for MO_2Cl_2 shown in Figure 10b argues that MoO_2Cl_2 is a volatile etch product. Another possible reaction product, $MoOCl_4$, could have been expected from the thermochemical results shown in eq 5. $MoOCl_4$ should have produced ion signal intensities around m/z 254. However, $MoOCl_4$ was not detected during $SOCl_2$ exposures. The main reaction products during Mo ALE were SO_2 and MoO_2Cl_2.

Figure 11 displays the time-resolved QMS spectra obtained during the fourth and fifth Mo ALE cycles on Mo powder using sequential O_3 and $SOCl_2$ exposures at 200 °C. The O_3 exposures produce ion signal intensity at m/z 32. During the following $SOCl_2$ exposure, ion signal intensities are observed at m/z 32, 64, 118, and 200 corresponding to S^+ or O_2^+, SO_2^+, $SOCl_2^+$, and $MoO_2Cl_2^+$, respectively. The ion signal at m/z 32 can be either S^+ or O_2^+, or both, and this ion signal is a crack of $SOCl_2$ or SO_2.

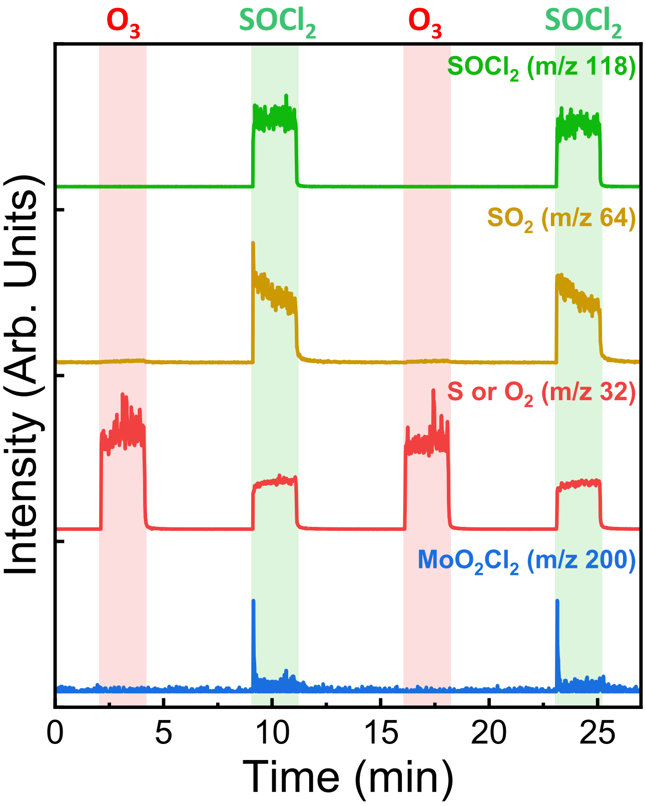

Figure 11. Time-resolved QMS spectra for Mo thermal ALE on Mo powder using sequential O_3 and $SOCl_2$ exposures at 200 °C. O_3 exposure is indicated by the light red-shaded region. $SOCl_2$ exposure is indicated by the light green-shaded region.

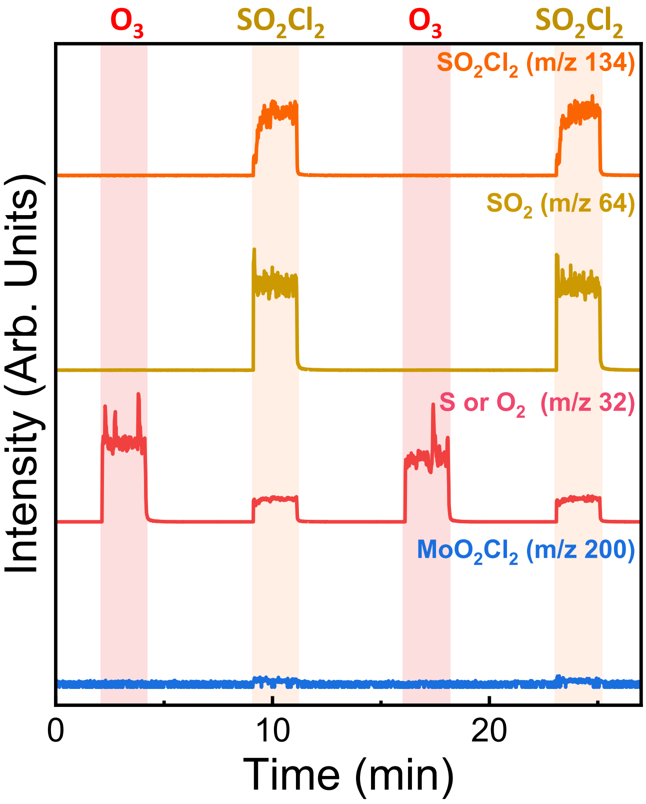

Figure 12. Time-resolved QMS spectra for Mo thermal ALE on Mo powder using sequential O_3 and SO_2Cl_2 exposures at 200 °C. O_3 exposure is indicated by the light red-shaded region. SO_2Cl_2 exposure is indicated by the light orange-shaded region.

The ion signal at m/z 64 is SO_2^+ that is produced according to eq 2. The ion signal at m/z 118 is attributed to $SOCl_2^+$ from the $SOCl_2$ reactant. The ion signal at m/z 200 corresponds to $MoO_2Cl_2^+$. MoO_2Cl_2 is a product of the reaction between $SOCl_2$ and MoO_3, according to eq 6. The reaction between $SOCl_2$ and MoO_3 is a deoxychlorination reaction. $SOCl_2$ accepts one oxygen atom from MoO_3 and donates two chlorine atoms to MoO_3, leading to the formation of SO_2 and MoO_2Cl_2.

The reactions between Mo powder and sequential O_3 and $SOCl_2$ exposures in Figure 11 can be compared with the reactions between Mo powder and sequential O_3 and SO_2Cl_2 exposures. Figure 12 displays the time-resolved QMS spectra obtained during the fourth and fifth Mo ALE cycles on Mo powder using sequential O_3 and SO_2Cl_2 exposures at 200 °C. The detected species are similar to the species observed in Figure 11 except that $SO_2Cl_2^+$ from the SO_2Cl_2 reactant is monitored at m/z 134. In addition, the time-resolved QMS results reveal that the $MoO_2Cl_2^+$ ion signal is not observed at m/z 200.

The lack of an ion signal for $MoO_2Cl_2^+$ in Figure 12 confirms that Mo ALE does not occur using sequential O_3 and SO_2Cl_2 exposures. Ion signals for $MoOCl_4^+$ at m/z 254 or $MoOCl_3^+$ at m/z 219 were also not observed during SO_2Cl_2 exposures on Mo powder during O_3 exposures. These results are in agreement with the QCM results in Figure 1 that showed no Mo ALE using sequential O_3 and SO_2Cl_2 exposures. In contrast, time-resolved QMS experiments on MoO_2 powder revealed MoO_2Cl_2 as an etch product using SO_2Cl_2 as the chlorination reactant. These results indicate that SO_2Cl_2 can etch MoO_2. The reaction between SO_2Cl_2 and MoO_2 is a chlorination reaction where SO_2Cl_2 donates two chlorine atoms to MoO_2 leading to the formation of SO_2 and MoO_2Cl_2.

III.IV. Roughness of Mo Surface versus Mo ALE Cycles.

AFM was used to characterize the roughness of the Mo surface versus Mo ALE cycles. Figure 13 displays the AFM images of the as-deposited Mo films immediately after preparation by Mo PVD and the Mo films etched using 100, 200, 300, and 400 ALE cycles. The RMS roughness of the Mo surface versus Mo ALE cycles is shown in Figure 14. The as-deposited Mo film had an RMS roughness of 6.2 ± 0.5 Å. After 100, 200, 300, and 400 cycles of Mo ALE, the RMS roughness gradually increased to 6.8, 9.5, 14.5, and 22.2 Å, respectively. These RMS roughness values all have a standard deviation of ±0.3 Å.

The increase in Mo surface roughness versus the number of ALE cycles can be caused by the polycrystalline nature of the Mo film. The as-deposited Mo PVD films displayed XRD peaks at 40.5, 58.6, and 73.5°.[64] These XRD peaks are consistent with the body-centered cubic Mo unit cell. The roughness increase with a larger number of ALE cycles may result from the different etch rates of the various crystalline facets.[28,32]

III.V. ALE of Other Metals Using Sequential Oxidation and Deoxychlorination Reactions.

Sequential oxidation and deoxychlorination reactions can also be employed for the ALE of other metals that have volatile oxychlorides. Metals with volatile oxychlorides include V, Nb, and Ta in Group 5 and Cr, Mo, and W in Group 6. These metals incorporate Mo from the current study and W from earlier studies.[31] The oxidation of these metals will produce V_2O_5, Nb_2O_5, Ta_2O_5, CrO_3, MoO_3, and WO_3. These metal oxides can then be reacted with the $SOCl_2$

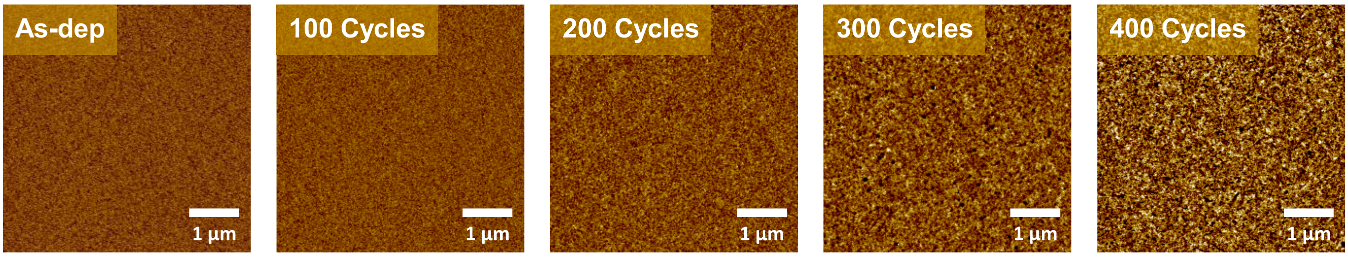

Figure 13. AFM images of Mo surface versus the number of Mo thermal ALE cycles at 150 °C.

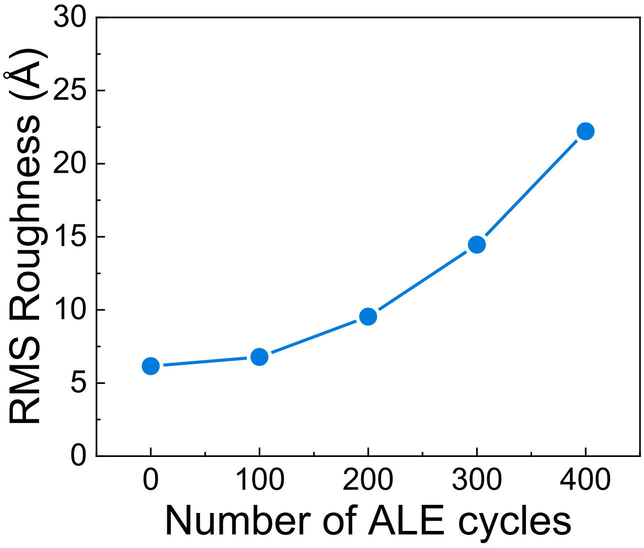

Figure 14. RMS roughness of Mo films versus number of Mo thermal ALE cycles at 150 °C.

deoxychlorination reactant to produce various volatile oxychlorides.

The thermochemistry of these deoxychlorination reactions is favorable. The predicted changes in standard Gibbs free energy at 300 °C for the various reactions between the metal oxide and $SOCl_2$ are given below[58]

$$V_2O_5 + 3SOCl_2(g) \rightarrow 2VOCl_3(g) + 3SO_2(g) \qquad \Delta G^\circ = -73\ \text{kcal} \tag{7}$$

$$Nb_2O_5 + 3SOCl_2(g) \rightarrow 2NbOCl_3(g) + 3SO_2(g) \qquad \Delta G^\circ = -20\ \text{kcal} \tag{8}$$

$$Ta_2O_5 + 3SOCl_2(g) \rightarrow 2TaOCl_3(g) + 3SO_2(g) \qquad \Delta G^\circ = -1\ \text{kcal} \tag{9}$$

$$CrO_3 + SOCl_2(g) \rightarrow CrO_2Cl_2(g) + SO_2(g) \qquad \Delta G^\circ = -35\ \text{kcal} \tag{10}$$

$$MoO_3 + SOCl_2(g) \rightarrow MoO_2Cl_2(g) + SO_2(g) \qquad \Delta G^\circ = -21\ \text{kcal} \tag{11}$$

$$WO_3 + SOCl_2(g) \rightarrow WO_2Cl_2(g) + SO_2(g) \qquad \Delta G^\circ = -8\ \text{kcal} \tag{12}$$

All of the predicted standard Gibbs free energy changes are negative. These results forecast spontaneous reactions under standard conditions if the reactions are not limited by activation barriers. These deoxychlorination reactions should enable thermal ALE of a large number of metals in addition to Mo.

IV. CONCLUSIONS

Mo thermal ALE was achieved based on sequential oxidation and deoxychlorination reactions with O_3 and $SOCl_2$ as the reactants. Using Mo-coated QCM crystals, in situ QCM studies revealed that the sequential O_3 and $SOCl_2$ exposures were able to etch Mo over a temperature range from 75 to 225 °C. The QCM results showed a linear mass decrease versus ALE cycles after a short etching delay. Every O_3 exposure led to a distinct mass increase. Every $SOCl_2$ exposure displayed a large mass decrease. The mass change during each $SOCl_2$ reactant exposure was self-limiting. The mass change during the O_3 exposure time displayed a soft saturation consistent with the diffusion-limited oxidation of Mo.

The Mo etch rate was dependent on temperature. The Mo etch rates were 0.94, 5.77, 8.83, and 10.98 Å/cycle at 75, 125, 175, and 225 °C, respectively, under saturation conditions. XPS measurements revealed MoO_3 on the Mo surface after O_3 exposure at 150 °C. SO_2 and MoO_2Cl_2 were detected when Mo was exposed to $SOCl_2$ during the Mo ALE cycles at 200 °C. These results are consistent with Mo ALE occurring by oxidation and deoxychlorination reactions. In this mechanism, Mo is oxidized to MoO_3 by O_3. Subsequently, MoO_3 undergoes a deoxychlorination reaction with $SOCl_2$ where $SOCl_2$ accepts oxygen to produce SO_2 and donates chlorine to yield MoO_2Cl_2.

To test this deoxychlorination mechanism, QCM experiments also monitored sequential exposures of O_3 and SO_2Cl_2 with Mo at 250 °C. These QCM results revealed that SO_2Cl_2 did not etch Mo. Mo thermal ALE requires a deoxychlorination reactant that can both accept oxygen from the metal oxide and donate chlorine to the metal oxide. Time-resolved QMS studies at 200 °C confirmed the volatile release of MoO_2Cl_2 only using the $SOCl_2$ deoxychlorination reactant. Mo thermal ALE was also observed to progressively roughen the Mo surface.

The oxidation and deoxychlorination reaction mechanism for metal thermal ALE should be useful for a variety of metals that have volatile oxychlorides. These metals include V, Nb, and Ta from Group 5 and Cr, Mo, and W from Group 6. These metals will add to the growing number of metals that can currently be etched using thermal ALE methods. This mechanism based on oxidation and deoxychlorination will complement the earlier mechanisms for metal thermal ALE based on either chlorination and ligand addition, or oxidation/chlorination followed by ligand substitution and hydrogen transfer reactions.

■ ASSOCIATED CONTENT

Supporting Information

The Supporting Information is available free of charge at https://pubs.acs.org/doi/10.1021/acs.chemmater.3c02606.

XPS survey spectra of PVD Mo with and without Ar^+ sputtering (PDF)

AUTHOR INFORMATION

Corresponding Author

Steven M. George — *Department of Chemistry, University of Colorado, Boulder, Colorado 80309, United States;* orcid.org/0000-0003-0253-9184; Email: Steven.George@Colorado.edu

Authors

Taewook Nam — *Department of Chemistry, University of Colorado, Boulder, Colorado 80309, United States;* orcid.org/0000-0001-9702-0873

Troy A. Colleran — *Department of Chemistry, University of Colorado, Boulder, Colorado 80309, United States*

Jonathan L. Partridge — *Department of Chemistry, University of Colorado, Boulder, Colorado 80309, United States;* orcid.org/0000-0002-0071-9854

Andrew S. Cavanagh — *Department of Chemistry, University of Colorado, Boulder, Colorado 80309, United States;* orcid.org/0000-0002-6201-530X

Complete contact information is available at: https://pubs.acs.org/10.1021/acs.chemmater.3c02606

Notes

The authors declare no competing financial interest.

ACKNOWLEDGMENTS

This work was supported in part by the Joint University Microelectronics Program (JUMP) funded by the Semiconductor Research Corporation (SRC). Funding for the QMS reactor and the QMS investigations was provided by Lam Research. The authors thank TMEiC for the use of the O_3 generator. The authors also thank Rebecca Hirsch for the XRD and XRR measurements.

REFERENCES

(1) Fischer, A.; Routzahn, A.; George, S. M.; Lill, T. Thermal Atomic Layer Etching: A Review. *J. Vac. Sci. Technol. A* **2021**, *39*, No. 030801.

(2) George, S. M. Mechanisms of Thermal Atomic Layer Etching. *Acc. Chem. Res.* **2020**, *53*, 1151−1160.

(3) Kanarik, K. J.; Lill, T.; Hudson, E. A.; Sriraman, S.; Tan, S.; Marks, J.; Vahedi, V.; Gottscho, R. A. Overview of Atomic Layer Etching in the Semiconductor Industry. *J. Vac. Sci. Technol. A* **2015**, *33*, No. 020802.

(4) Lee, Y.; George, S. M. Atomic Layer Etching of Al_2O_3 Using Sequential, Self-Limiting Thermal Reactions with $Sn(acac)_2$ and Hydrogen Fluoride. *ACS Nano* **2015**, *9*, 2061−2070.

(5) George, S. M.; Lee, Y. Prospects for Thermal Atomic Layer Etching Using Sequential, Self-Limiting Fluorination and Ligand-Exchange Reactions. *ACS Nano* **2016**, *10*, 4889−4894.

(6) Lee, Y.; DuMont, J. W.; George, S. M. Trimethylaluminum as the Metal Precursor for the Atomic Layer Etching of Al_2O_3 Using Sequential, Self-Limiting Thermal Reactions. *Chem. Mater.* **2016**, *28*, 2994−3003.

(7) Lee, Y.; George, S. M. Thermal Atomic Layer Etching of Al_2O_3, HfO_2, and ZrO_2 Using Sequential Hydrogen Fluoride and Dimethylaluminum Chloride Exposures. *J. Phys. Chem. C* **2019**, *123*, 18455−18466.

(8) Murdzek, J. A.; Rajashekhar, A.; Makala, R. S.; George, S. M. Thermal Atomic Layer Etching of Amorphous and Crystalline Al_2O_3 Films. *J. Vac. Sci. Technol. A* **2021**, *39*, No. 042602.

(9) Reif, J.; Knaut, M.; Killge, S.; Albert, M.; Mikolajick, T.; Bartha, J. W. In situ Studies on Atomic Layer Etching of Aluminum Oxide Using Sequential Reactions with Trimethylaluminum and Hydrogen Fluoride. *J. Vac. Sci. Technol. A* **2022**, *40*, No. 032602.

(10) Lee, Y.; George, S. M. Thermal Atomic Layer Etching of HfO_2 Using HF for Fluorination and $TiCl_4$ for Ligand-Exchange. *J. Vac. Sci. Technol. A* **2018**, *36*, No. 061504.

(11) Lee, Y.; DuMont, J. W.; George, S. M. Atomic Layer Etching of HfO_2 Using Sequential, Self-Limiting Thermal Reactions with $Sn(acac)_2$ and HF. *ECS J. Solid State Sci. Technol.* **2015**, *4*, N5013−N5022.

(12) Murdzek, J. A.; George, S. M. Effect of Crystallinity on Thermal Atomic Layer Etching of Hafnium Oxide, Zirconium Oxide, and Hafnium Zirconium Oxide. *J. Vac. Sci. Technol. A* **2020**, *38*, No. 022608.

(13) Lee, Y.; Huffman, C.; George, S. M. Selectivity in Thermal Atomic Layer Etching Using Sequential, Self Limiting Fluorination and Ligand-Exchange Reactions. *Chem. Mater.* **2016**, *28*, 7657−7665.

(14) Zywotko, D. R.; Zandi, O.; Faguet, J.; Abel, P. R.; George, S. M. ZrO_2 Monolayer as a Removable Etch Stop Layer for Thermal Al_2O_3 Atomic Layer Etching Using Hydrogen Fluoride and Trimethylaluminum. *Chem. Mater.* **2020**, *32*, 10055−10065.

(15) Lee, Y.; Johnson, N. R.; George, S. M. Thermal Atomic Layer Etching of Gallium Oxide Using Sequential Exposures of HF and Various Metal Precursors. *Chem. Mater.* **2020**, *32*, 5937−5948.

(16) Johnson, N. R.; Hite, J. K.; Mastro, M. A.; Eddy, C. R.; George, S. M. Thermal Atomic Layer Etching of Crystalline GaN Using Sequential Exposures of XeF_2 and BCl_3. *Appl. Phys. Lett.* **2019**, *114*, No. 243103.

(17) Cano, A. M.; Lii-Rosales, A.; George, S. M. Thermal Atomic Layer Etching of Aluminum Nitride Using HF or XeF_2 for Fluorination and BCl_3 for Ligand Exchange. *J. Phys. Chem. C* **2022**, *126*, 6990−6999.

(18) Johnson, N. R.; Sun, H. X.; Sharma, K.; George, S. M. Thermal Atomic Layer Etching of Crystalline Aluminum Nitride Using Sequential, Self-Limiting Hydrogen Fluoride and $Sn(acac)_2$ Reactions and Enhancement by H_2 and Ar Plasmas. *J. Vac. Sci. Technol. A* **2016**, *34*, No. 050603.

(19) DuMont, J. W.; Marquardt, A. E.; Cano, A. M.; George, S. M. Thermal Atomic Layer Etching of SiO_2 by a "Conversion-Etch" Mechanism Using Sequential Reactions of Trimethylaluminum and Hydrogen Fluoride. *ACS Appl. Mater. Interfaces* **2017**, *9*, 10296−10307.

(20) Zywotko, D. R.; George, S. M. Thermal Atomic Layer Etching of ZnO by a "Conversion-Etch" Mechanism Using Sequential Exposures of Hydrogen Fluoride and Trimethylaluminum. *Chem. Mater.* **2017**, *29*, 1183−1191.

(21) Gertsch, J. C.; Partridge, J. L.; Cano, A. M.; Clancey, J. W.; Bright, V. M.; George, S. M. Thermal Atomic Layer Etching of VO_2 Using Sequential BCl_3 and SF_4 Exposures: Observation of Conversion, Ligand-Exchange, and Oxidation State Changes. *J. Vac. Sci. Technol. A* **2023**, *41*, No. 012603.

(22) Cano, A. M.; Partridge, J. L.; George, S. M. Thermal Atomic Layer Etching of Al_2O_3 Using Sequential HF and BCl_3 Exposures: Evidence for Combined Ligand-Exchange and Conversion Mechanisms. *Chem. Mater.* **2022**, *34*, 6440−6449.

(23) Lee, Y.; George, S. M. Thermal Atomic Layer Etching of Titanium Nitride Using Sequential, Self-Limiting Reactions: Oxidation to TiO_2 and Fluorination to Volatile TiF_4. *Chem. Mater.* **2017**, *29*, 8202−8210.

(24) Abdulagatov, A. I.; George, S. M. Thermal Atomic Layer Etching of Silicon Using O_2, HF, and $Al(CH_3)_3$ as the Reactants. *Chem. Mater.* **2018**, *30*, 8465−8475.

(25) Abdulagatov, A. I.; Sharma, V.; Murdzek, J. A.; Cavanagh, A. S.; George, S. M. Thermal Atomic Layer Etching of Germanium-Rich SiGe Using an Oxidation and ″Conversion-Etch″ Mechanism. *J. Vac. Sci. Technol. A* **2021**, *39*, No. 022602.

(26) Abdulagatov, A. I.; George, S. M. Thermal Atomic Layer Etching of Silicon Nitride Using an Oxidation and ″Conversion Etch″ Mechanism. *J. Vac. Sci. Technol. A* **2020**, *38*, No. 022607.

(27) Lee, Y.; DuMont, J. W.; George, S. M. Atomic Layer Etching of AlF_3 Using Sequential, Self-Limiting Thermal Reactions with $Sn(acac)_2$ and Hydrogen Fluoride. *J. Phys. Chem. C* **2015**, *119*, 25385−25393.

(28) Nam, T.; Partridge, J. L.; George, S. M. Thermal Atomic Layer Etching of Zinc Sulfide Using Sequential Trimethylaluminum and

Hydrogen Fluoride Exposures: Evidence for a Conversion Mechanism. *Chem. Mater.* **2023**, *35*, 6671−6681.

(29) Johnson, N. R.; George, S. M. WO_3 and W Thermal Atomic Layer Etching Using "Conversion-Fluorination" and "Oxidation-Conversion-Fluorination" Mechanisms. *ACS Appl. Mater. Interfaces* **2017**, *9*, 34435−34447.

(30) Xie, W. Y.; Lemaire, P. C.; Parsons, G. N. Thermally Driven Self-Limiting Atomic Layer Etching of Metallic Tungsten Using WF_6 and O_2. *ACS Appl. Mater. Interfaces* **2018**, *10*, 9147−9154.

(31) Xie, W. Y.; Parsons, G. N. Thermal Atomic layer Etching of Metallic Tungsten via Oxidation and Etch Reaction Mechanism Using O_2 or O_3 for Oxidation and WCl_6 as the Chlorinating Etchant. *J. Vac. Sci. Technol. A* **2020**, *38*, No. 022605.

(32) Murdzek, J. A.; Lii-Rosales, A.; George, S. M. Thermal Atomic Layer Etching of Nickel Using Sequential Chlorination and Ligand-Addition Reactions. *Chem. Mater.* **2021**, *33*, 9174−9183.

(33) Murdzek, J. A.; Lii-Rosales, A.; George, S. M. Thermal Atomic Layer Etching of Cobalt Using Sulfuryl Chloride for Chlorination and Tetramethylethylenediamine or Trimethylphosphine for Ligand Addition. *J. Vac. Sci. Technol. A* **2023**, *41*, No. 032603.

(34) Mohimi, E.; Chu, X. Q. I.; Trinh, B. B.; Babar, S.; Girolami, G. S.; Abelson, J. R. Thermal Atomic Layer Etching of Copper by Sequential Steps Involving Oxidation and Exposure to Hexafluoroacetylacetone. *ECS J. Solid State Sci. Technol.* **2018**, *7*, P491−P495.

(35) Konh, M.; He, C.; Lin, X.; Guo, X. Y.; Pallem, V.; Opila, R. L.; Teplyakov, A. V.; Wang, Z. J.; Yuan, B. Molecular Mechanisms of Atomic Layer Etching of Cobalt with Sequential Exposure to Molecular Chlorine and Diketones. *J. Vac. Sci. Technol. A* **2019**, *37*, No. 021004.

(36) Wang, Z. J.; Opila, R. L. In Operando X-ray Photoelectron Spectroscopy Study of Mechanism of Atomic Layer Etching of Cobalt. *J. Vac. Sci. Technol. A* **2020**, *38*, No. 022611.

(37) George, M. A.; Hess, D. W.; Beck, S. E.; Ivankovits, J. C.; Bohling, D. A.; Lane, A. P. Reaction of 1,1,1,5,5,5-Hexafluoro-2,4-Pentanedione (Hhfac) With CuO, Cu_2O, and Cu Films. *J. Electrochem. Soc.* **1995**, *142*, 961−965.

(38) Jain, A.; Kodas, T. T.; Hampden-Smith, M. J. Thermal Dry-Etching of Copper Using Hydrogen Peroxide and Hexafluoroacetylacetone. *Thin Solid Films* **1995**, *269*, 51−56.

(39) Kang, S. W.; Kim, H. U.; Rhee, S. W. Dry Etching of Copper Film with Hexafluoroacetylacetone via Oxidation Process. *J. Vac. Sci. Technol. B* **1999**, *17*, 154−157.

(40) Steger, R.; Masel, R. Chemical Vapor Etching of Copper Using Oxygen and 1,1,1,5,5,5-Hexafluoro-2,4-Pentanedione. *Thin Solid Films* **1999**, *342*, 221−229.

(41) Chen, J. K. C.; Altieri, N. D.; Kim, T.; Chen, E.; Lill, T.; Shen, M. H.; Chang, J. P. Directional Etch of Magnetic and Noble Metals. II. Organic Chemical Vapor Etch. *J. Vac. Sci. Technol. A* **2017**, *35*, No. 05c305.

(42) Wadsworth, J.; Nieh, T. G.; Stephens, J. J. Recent Advances in Aerospace Refractory Metal Alloys. *Int. Mater. Rev.* **1988**, *33*, 131−150.

(43) Gall, D. Electron Mean Free Path in Elemental Metals. *J. Appl. Phys.* **2016**, *119*, No. 085101.

(44) Founta, V.; Soulié, J.-P.; Sankaran, K.; Vanstreels, K.; Opsomer, K.; Morin, P.; Lagrain, P.; Franquet, A.; Vanhaeren, D.; Conard, T.; et al. Properties of Ultrathin Molybdenum Films for Interconnect Applications. *Materialia* **2022**, *24*, No. 101511.

(45) Preist, R. C. Gaseous Precision Etching of Molybdenum. *US Govt. Res. Dev. Rep* **1966**, *67*, 98.

(46) Pacco, A.; Nakano, T.; Iwahata, S.; Iwasaki, A.; Sanchez, E. A. Etching of Molybdenum via a Combination of Low-Temperature Ozone Oxidation and Wet-Chemical Oxide Dissolution. *J. Vac. Sci. Technol. A* **2023**, *41*, No. 032601.

(47) Fischl, D. S.; Hess, D. W. Molybdenum Etching with Chlorine Atoms and Molecular Chlorine Plasmas. *J. Vac. Sci. Technol. B* **1988**, *6*, 1577−1580.

(48) Kurogi, Y.; Kamimura, K. Molybdenum Etching Using CCl_4/O_2 Mixture Gas. *Jpn. J. Appl. Phys.* **1982**, *21*, 168.

(49) Kim, Y.; Kang, H.; Ha, H.; Kim, C.; Cho, S.; Chae, H. Plasma Atomic Layer Etching of Molybdenum with Surface Fluorination. *Appl. Surf. Sci.* **2023**, *627*, No. 157309.

(50) Lee, Y.; Kim, Y.; Son, J.; Chae, H. Low-Temperature Plasma Atomic Layer Etching of Molybdenum via Sequential Oxidation and Chlorination. *J. Vac. Sci. Technol. A* **2022**, *40*, No. 022602.

(51) Elam, J. W.; Groner, M. D.; George, S. M. Viscous Flow Reactor with Quartz Crystal Microbalance for Thin Film Growth by Atomic Layer Deposition. *Rev. Sci. Instrum.* **2002**, *73*, 2981−2987.

(52) Wagner, C. D.; Wagner, C. D.; Muilenberg, G. E. *Handbook of X-ray Photoelectron Spectroscopy: A Reference Book of Standard Data for Use in X-ray Photoelectron Spectroscopy*; Perkin-Elmer, 1979.

(53) Major, G. H.; Fairley, N.; Sherwood, P. M. A.; Linford, M. R.; Terry, J.; Fernandez, V.; Artyushkova, K. Practical Guide for Curve Fitting in X-Ray Photoelectron Spectroscopy. *J. Vac. Sci. Technol. A* **2020**, *38*, No. 061203.

(54) Partridge, J. L.; Murdzek, J. A.; Johnson, V. L.; Cavanagh, A. S.; Fischer, A.; Lill, T.; Sharma, S.; George, S. M. Thermal Atomic Layer Etching of CoO, ZnO, Fe_2O_3, and NiO by Chlorination and Ligand Addition Using SO_2Cl_2 and Tetramethylethylenediamine. *Chem. Mater.* **2023**, *35*, 2058−2068.

(55) Lii-Rosales, A.; Cavanagh, A. S.; Fischer, A.; Lill, T.; George, S. M. Spontaneous Etching of Metal Fluorides Using Ligand-Exchange Reactions: Landscape Revealed by Mass Spectrometry. *Chem. Mater.* **2021**, *33*, 7719−7730.

(56) Baltrusaitis, J.; Mendoza-Sanchez, B.; Fernandez, V.; Veenstra, R.; Dukstiene, N.; Roberts, A.; Fairley, N. Generalized Molybdenum Oxide Surface Chemical State XPS Determination via Informed Amorphous Sample Model. *Appl. Surf. Sci.* **2015**, *326*, 151−161.

(57) Choi, J. G.; Thompson, L. T. XPS Study of As-Prepared and Reduced Molybdenum Oxides. *Appl. Surf. Sci.* **1996**, *93*, 143−149.

(58) HSC Chemisty *HSC Chemistry 9.9.2.3, Outokumpu Research Oy: Pori, Finland*.

(59) Deal, B. E.; Grove, A. S. General Relationship for the Thermal Oxidation of Silicon. *J. Appl. Phys.* **1965**, *36*, 3770−3778.

(60) Zhang, Y.; Li, C.; Cai, K.; Chen, Y.; Chen, S.; Lai, H.; Kang, J. Experimental Evidence of Oxidant-Diffusion-Limited Oxidation of SiGe Alloys. *J. Appl. Phys.* **2009**, *106*, No. 063508.

(61) Crist, B. V. *Handbook of Monochromatic XPS Spectra: The Elements of Native Oxides*; John Wiley & Sons, 2000.

(62) NIST. *Standard Reference Database 69: NIST Chemistry WebBook*, 2021.

(63) Hoefs, J. *Stable Isotope Geochemistry*; Springer, 1997.

(64) Yadav, P. K.; Sant, T.; Mukherjee, C.; Nayak, M.; Rai, S. K.; Lodha, G. S.; Sharma, S. M. Influence of Ion-To-Atom Ratio on the Microstructure of Evaporated Molybdenum Thin Films Grown Using Low Energy Argon Ions. *J. Vac. Sci. Technol. A* **2014**, *32*, No. 021509.